

Lead Free Alloyed Double Perovskites: An Emerging Class of Materials from Many-Body Perturbation Theory

Manjari Jain,* Manish Kumar, Preeti Bhumla, and Saswata Bhattacharya*

Department of Physics, Indian Institute of Technology Delhi, New Delhi, India

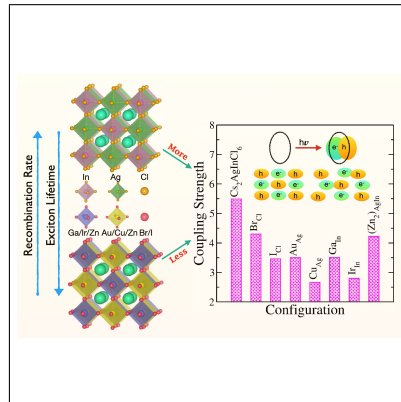
E-mail: Manjari.Jain@physics.iitd.ac.in[MJ]; saswata@physics.iitd.ac.in[SB]

Phone: +91-11-2659 1359

Abstract

The discovery of lead free all-inorganic alloyed double perovskites have revolutionized photovoltaic research, showing promising light emitting efficiency and its tunability. However, detailed studies regarding optical, exciton, polaron and transport properties remain unexplored. Here, we report a theoretical study on the variation of carrier-lattice interaction and optoelectronic properties of pristine as well as alloyed $\text{Cs}_2\text{AgInCl}_6$ double perovskites. We have employed many-body perturbation theory ($G_0W_0@HSE06$) and density functional perturbation theory (DFPT) to compute exciton binding energy (E_B) and exciton lifetime of different alloyed double perovskites. We find that phonon scattering limits charge-carrier mobilities and thus, plays an important role in the development of high-efficiency perovskite photovoltaics. In view of this, dominant carrier-phonon scattering is observed via Fröhlich mechanism near room temperature. Moreover, we observe a noticeable increase in hole and electron mobilities on alloying. We believe that our results will be helpful to gain a better understanding of the optoelectronic properties and lattice dynamics of these double perovskites.

Graphical TOC Entry



In a remarkably short period of time, lead halide perovskites have emerged in an unprecedented way in the field of optoelectronics by virtue of their exceptional properties like suitable optical band gap, long carrier diffusion length, high carrier mobility and low manufacturing cost¹⁻⁹. The power conversion efficiency of lead halide perovskites-based solar cells has increased from 3.8% to 25.5% in the last decade^{10,11}. Despite their great potential, there are two major challenges including Pb toxicity and phase instability. The stability issues have been partly overcome by replacing organic cation with inorganic cesium ion^{12,13}. However, Pb toxicity is still a drawback and dealing with this issue without compromising the efficiency is of paramount importance.

Over the past few years, lead free all-inorganic double perovskites with formula $A_2B'B''X_6$ have emerged as possible contenders due to low toxicity, intrinsic thermodynamic stability and small carrier effective mass¹⁴⁻²³. In particular, the double perovskite $Cs_2AgInCl_6$ has been the subject of several studies, revealing excellent environmental stability and promising optoelectronic properties. For example, $Cs_2AgInCl_6$ double perovskite exhibits a direct band gap as well as ultralong carrier lifetime (6 μs), which are suitable for photovoltaic applications^{24,25}. Moreover, Luo *et al.* reported that the alloying of Na cation in double perovskite $Cs_2AgInCl_6$ increases the photoluminescence efficiency by three orders and emits a warm white light with enhanced quantum efficiency²⁶. Also, $Cs_2AgInCl_6$ has found to be successfully synthesized experimentally with the direct band gap of 3.3 eV and good stability²⁷. However, the wide band gap of $Cs_2AgInCl_6$ doesn't show optical response in visible region. In order to reduce its band gap and expand the spectral response in visible light region, alloying with suitable elements could be the best solution. In one of our recent works, we have done the sublattice mixing by partial substitution of several metals M(I), M(II), M(III), and halogen X at Ag/In and Cl sites, respectively, to reduce the band gap of $Cs_2AgInCl_6$ and hence, enhancing its optical properties²⁸. We have found that sublattices with Br and I substitutions at the Cl site, Cu(I) and Au(I) at the Ag site, Ga and Ir(III) at the In site, and Zn(II) at the Ag and In sites simultaneously have tuned the band gap in the visible region. In the present work, we have studied the excitonic properties and the role of electron-phonon coupling in these promising perovskites.

Formation of excitons in optoelectronic materials greatly influences the charge separation properties. Hence, accurate estimation of excitonic parameters viz. exciton binding energy, exciton radius and exciton lifetime is of great importance in this class of materials. The excitons dissociate into free charge carriers, which effect the solar cell performance. Moreover, in order to explain multiple photophysical phenomena in perovskite materials, the concept of polarons has been used. The polaronic effect plays a crucial role in the excitaion dynamics and charge transport. The separation of free charge carriers is also influenced by the carrier mobility, which in turn depends on the electron-phonon (e-ph) coupling strength. Understanding the effect of electron-phonon coupling in terms of polaron mobility is important. In view of this, we attempt here to explore electronic and optical properties of $\text{Cs}_2\text{AgInCl}_6$ and its alloyed counterparts using state-of-the-art many-body perturbation theory. Various important aspects such as excitonic properties, carrier mobility, the role of electron-phonon coupling have been studied presumably for the first time in this class of materials. Using Fröhlich model, we have also discussed the effect of electron-phonon coupling and calculated the polaron mobility.

According to Wannier-Mott model²⁹, the exciton binding energy (E_B) for screened interacting electron-hole (e-h) pair is given by:

$$E_B = \left(\frac{\mu}{\epsilon_{\text{eff}}^2} \right) R_{\infty} \quad (1)$$

where, μ is the reduced mass, ϵ_{eff} is the effective dielectric constant and R_{∞} is the Rydberg con-

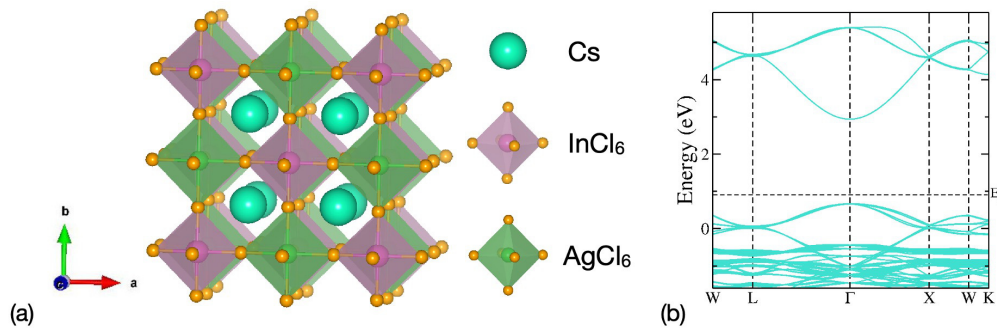


Figure 1: (a) Crystal structure of $\text{Cs}_2\text{AgInCl}_6$ double perovskite and (b) bandstructure of $\text{Cs}_2\text{AgInCl}_6$ using $G_0W_0@HSE06$. E_f is fermi energy level.

stant. In order to compute E_B , firstly we have calculated the effective mass of electrons and holes using Wannier-Mott approach by plotting E - k dispersion curve (see Fig. 1(b) for pristine $\text{Cs}_2\text{AgInCl}_6$ and for different alloyed compounds, see section I of supplementary information (SI)). The conduction band minimum (CBm) and valence band maximum (VBM) are obtained at high symmetry point Γ (0, 0, 0). We have done the parabolic fitting of the dispersion curves for calculating the effective mass of the electrons and holes. Further, we have taken the average of effective mass values from $\Gamma \rightarrow \text{L}$ and $\Gamma \rightarrow \text{X}$ directions. The effective mass can be calculated by using expression:

$$m^* = \frac{\hbar^2}{\frac{d^2E(k)}{dk^2}} \quad (2)$$

where m^* , $E(k)$, k , and \hbar are the effective mass, energy, wave vector and reduced Planck's constant, respectively. The calculated effective mass and reduced mass in terms of rest mass of electron (m_0) for pristine $\text{Cs}_2\text{AgInCl}_6$ double perovskite and different alloyed compounds are listed in Table 1. The obtained values of effective mass and reduced mass for $\text{Cs}_2\text{AgInCl}_6$ double perovskite are well in agreement with the previous findings³⁰.

Table 1: Effective mass of electron m_e^* , hole m_h^* and reduced mass μ in terms of rest mass of electron m_0 .

Compounds	m_e^*	m_h^*	μ
$\text{Cs}_2\text{AgInCl}_6$	0.29	1.07	0.23
$\text{Cs}_2\text{AgInBr}_{0.04}\text{Cl}_{5.96}$	0.28	0.80	0.21
$\text{Cs}_2\text{AgInI}_{0.04}\text{Cl}_{5.96}$	0.26	0.67	0.19
$\text{Cs}_2\text{Au}_{0.25}\text{Ag}_{0.75}\text{InCl}_6$	0.25	0.80	0.19
$\text{Cs}_2\text{Cu}_{0.25}\text{Ag}_{0.75}\text{InCl}_6$	0.27	1.09	0.22
$\text{Cs}_2\text{AgGa}_{0.25}\text{In}_{0.75}\text{Cl}_6$	0.27	0.84	0.21
$\text{Cs}_2\text{AgIr}_{0.25}\text{In}_{0.75}\text{Cl}_6$	0.29	0.86	0.22
$\text{Cs}_2\text{Zn}_{0.50}\text{Ag}_{0.75}\text{In}_{0.75}\text{Cl}_6$	0.28	0.83	0.21

Now, our next task is to compute ϵ_{eff} in order to find the exciton binding energy of pristine $\text{Cs}_2\text{AgInCl}_6$ and different alloyed compounds. As it is reported earlier that the E_B gets changed due

to the lattice relaxation³¹ i.e., if ω_{LO} is the longitudinal optical phonon frequency and $E_B \ll \hbar\omega_{LO}$, then one needs to consider lattice relaxation. Therefore, a value intermediate between the static electronic dielectric constant at high-frequency (ϵ_∞) and the static ionic dielectric constant at low frequency (ϵ_{static}) should be considered for the ϵ_{eff} . However, if $E_B \gg \hbar\omega_{LO}$ then the ionic contribution to the dielectric screening is negligible and, hence does not alter the E_B ³². In such cases, $\epsilon_{eff} \rightarrow \epsilon_\infty$, where ϵ_∞ is the static value of dielectric constant at high frequency that mainly consists of electronic contribution.

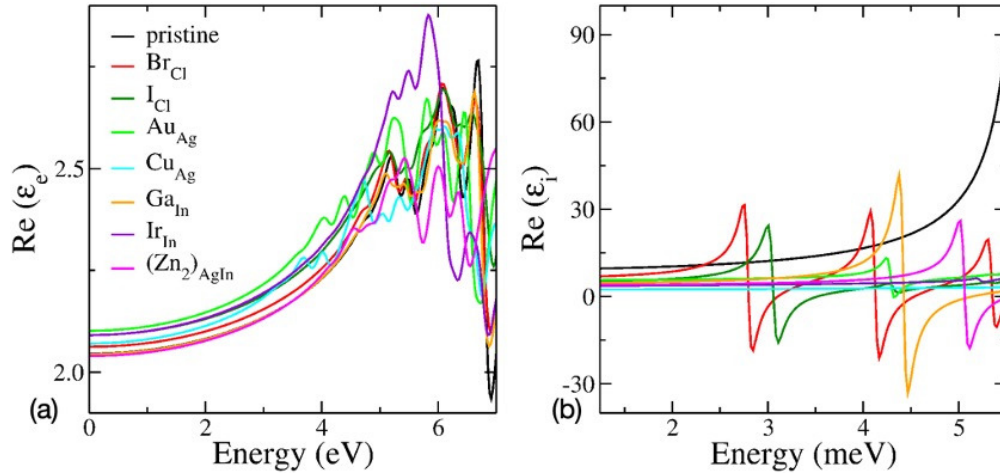


Figure 2: (a) Electronic contribution to the dielectric function and (b) ionic contribution to the dielectric function of pristine $Cs_2AgInCl_6$ and different alloyed compounds.

In Fig. 2(a), we have shown the electronic contribution of the dielectric function calculated using $G_0W_0@HSE06$ and in Fig. 2(b), we have plotted the ionic contribution to the dielectric function computed using DFPT approach. The value of ϵ_∞ and ϵ_{static} for pristine $Cs_2AgInCl_6$ double perovskite are 2.05 and 9.63, respectively, which are well in agreement with the obtained values in previous reports^{28,33}. Also from Fig. 2(b), we have observed that the value of ϵ_{static} for the alloyed compounds is less than the pristine $Cs_2AgInCl_6$, which implies that the ionic contribution to the dielectric constant in case of alloyed compounds is less prominent than the pristine $Cs_2AgInCl_6$. Now, using reduced mass (provided in Table 1) and the dielectric constants, we have determined the upper and lower bounds of E_B using Eq 1, listed in Table 2.

By knowing the exciton binding energy, dielectric function, and reduced mass, we can calculate

Table 2: Upper bound (E_{Bu}) and lower bound (E_{Bl}) on exciton binding energy E_B for double perovskites.

Compounds	ϵ_∞	E_{Bu} (eV)	ϵ_{static}	E_{Bl} (eV)
$Cs_2AgInCl_6$	2.05	0.74	9.63	0.03
$Cs_2AgInBr_{0.04}Cl_{5.96}$	2.06	0.67	6.90	0.06
$Cs_2AgInI_{0.04}Cl_{5.96}$	2.09	0.59	5.25	0.09
$Cs_2Au_{0.25}Ag_{0.75}InCl_6$	2.10	0.58	5.64	0.08
$Cs_2Cu_{0.25}Ag_{0.75}InCl_6$	2.07	0.70	3.71	0.21
$Cs_2AgGa_{0.25}In_{0.75}Cl_6$	2.05	0.68	4.71	0.12
$Cs_2AgIr_{0.25}In_{0.75}Cl_6$	2.09	0.87	3.72	0.27
$Cs_2Zn_{0.50}Ag_{0.75}In_{0.75}Cl_6$	2.05	0.68	4.01	0.17

the various excitonic parameters such as exciton radius (r_{exc}) and the probability of a wavefunction ($|\phi_n(0)|^2$) at zero charge separation (given in Table 3). The exciton radius (r_{exc}) is calculated as follows:

$$r_{exc} = \frac{m_0}{\mu} \epsilon_{eff} n^2 r_{Ry} \quad (3)$$

where m_0 is the free electron mass, μ is the reduced mass, ϵ_{eff} is the effective dielectric constant (here, the electronic dielectric constant has been taken), n is the exciton energy level ($n=1$ provides the smallest exciton radius) and $r_{Ry} = 0.0529$ nm is the Bohr radius. For electron-hole pair at zero separation, the exciton lifetime (τ) is inversely proportional to the probability of a wavefunction ($|\phi_n(0)|^2$). The $|\phi_n(0)|^2$ is determined as follows:

$$|\phi_n(0)|^2 = \frac{1}{\pi(r_{exc})^3 n^3} \quad (4)$$

From Table 3, it is observed that the alloyed compounds have longer exciton lifetime than the pristine $Cs_2AgInCl_6$ double perovskite. The longer exciton lifetime corresponds to lower recombination, which leads to higher quantum yield and conversion efficiency³⁴. Hence, the different alloyed compounds, having longer exciton lifetime than the pristine $Cs_2AgInCl_6$, are good for solar cells and photovoltaic devices.

Table 3: Excitonic parameters of Cs₂AgInCl₆ and different alloyed compounds.

Compounds	r _{exc} (nm)	φ _n (0) ² (10 ²⁷ m ⁻³)
Cs ₂ AgInCl ₆	0.47	2.96
Cs ₂ AgInBr _{0.04} Cl _{5.96}	0.53	2.18
Cs ₂ AgInI _{0.04} Cl _{5.96}	0.59	1.54
Cs ₂ Au _{0.25} Ag _{0.75} InCl ₆	0.56	1.81
Cs ₂ Cu _{0.25} Ag _{0.75} InCl ₆	0.50	2.54
Cs ₂ AgGa _{0.25} In _{0.75} Cl ₆	0.53	2.13
Cs ₂ AgIr _{0.25} In _{0.75} Cl ₆	0.49	2.87
Cs ₂ Zn _{0.50} Ag _{0.75} In _{0.75} Cl ₆	0.51	2.39

In order to calculate the charge carrier mobility, we have used deformation potential model proposed by Bardeen and Shockley³⁵. According to this model, the charge carrier mobility (μ) for 3D materials can be expressed as:

$$\mu = \frac{2\sqrt{2}\pi e\hbar^4 C_{3D}}{3(k_B T)^{3/2} (m^*)^{5/2} E_l^2} \quad (5)$$

where k_B is the Boltzmann constant, T is the temperature, and e is the elementary charge of electron (for more details, see section II of SI). We can see from Eq. 5, the effective mass has a significant effect on the carrier mobility. Due to the intrinsic cubic structure, the pristine Cs₂AgInCl₆ and different alloyed compounds show an isotropic transport character. From Table 1, it can be seen that the hole effective mass is nearly 3 times larger than that of the electron, which implies that electron transport ability is better than hole transport ability. Further, along with effective mass, the carrier mobility also depends on 3D elastic constant C_{3D} and deformation potential E_l . In order to compute C_{3D} and E_l , uniaxial strain has been applied along the lattice direction (z-axis). The total energies and positions of the VBM and CBm are calculated with respect to the uniaxial strain using PBE xc functional. These values are also calculated using HSE06 xc functional for Cs₂AgInCl₆ and Cs₂Cu_{0.25}Ag_{0.75}InCl₆, which are comparable with PBE xc functional (see section III of SI for comparison). Therefore, we have used PBE xc functional as it is computationally more cost effective. Now, C_{3D} can be obtained by fitting the energy vs strain curve and E_l is proportional to the

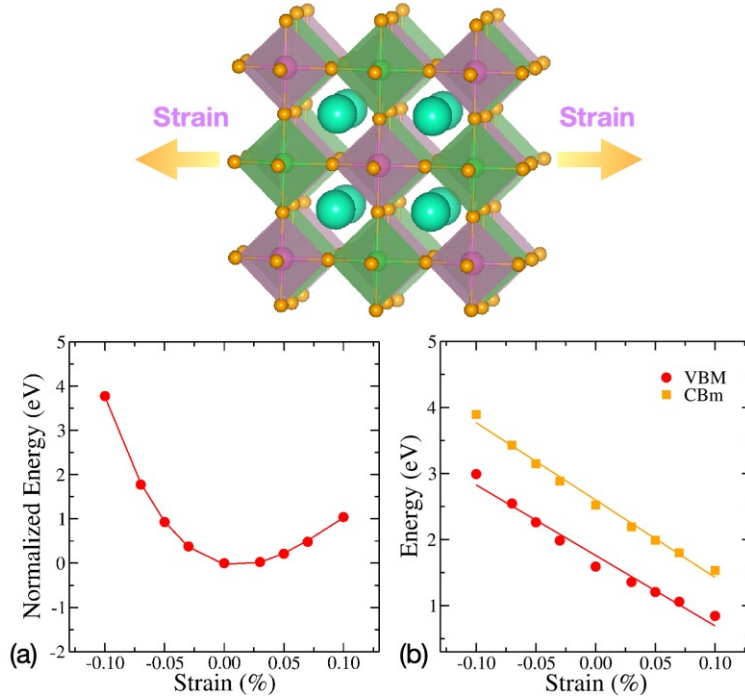


Figure 3: (a) Relationship between total energy and the applied strain along the transport direction (z-axis) (b) Band energy shifts of VBM and CBm under uniaxial strain for Cs₂AgInCl₆.

band edge shift induced by applied strain along the transport direction (see Fig. 3 for Cs₂AgInCl₆). Subsequently, based on the obtained values of m^* , C_{3D} and E_I , the electron mobility comes out to be $665.38 \text{ cm}^2\text{V}^{-1}\text{s}^{-1}$ and the hole mobility is $30.68 \text{ cm}^2\text{V}^{-1}\text{s}^{-1}$ for Cs₂AgInCl₆. The obtained hole mobility is quite well in agreement with the previous finding³⁶. Note that, the electron mobility is about 20 times higher than that of the hole mobility. Further, for the alloyed compounds, we have observed increment in carrier mobilities in comparison to pristine Cs₂AgInCl₆ (see Table 4). This demonstrates excellent photovoltaic properties for the alloyed compounds than the pristine (For more details of C_{3D} and E_I for alloyed compounds, see section IV in SI).

The influence of electron-phonon coupling on physical/chemical properties of a material remains an alluring paradox. It has been reported that in case of polar semiconductors (e.g., halide perovskites), the interaction of carriers with the macroscopic electric field generated by longitudinal optical (LO) phonons, known as the Fröhlich interaction is the dominating scattering mechanism near room temperature^{37,38}. In order to find the reason behind the discrepancy in mobility

Table 4: Calculated deformation potential constant (E_l), 3D elastic constant (C_{3D}), and carrier mobility (μ) for electrons and holes along the transport direction (z-axis) of different configurations at 300 K.

Compounds	Carrier type	E_l (eV)	C_{3D} (Nm ⁻²)	μ (cm ² V ⁻¹ s ⁻¹)
Cs ₂ AgInCl ₆	electron	11.71	67.48	665.38
	hole	10.66	67.48	30.68
Cs ₂ AgInBr _{0.04} Cl _{5.96}	electron	11.69	70.81	730.98
	hole	11.26	70.81	59.21
Cs ₂ AgInI _{0.04} Cl _{5.96}	electron	11.83	76.72	965.19
	hole	11.91	76.72	90.05
Cs ₂ Au _{0.25} Ag _{0.75} InCl ₆	electron	11.57	67.25	909.88
	hole	10.69	67.25	63.79
Cs ₂ Cu _{0.25} Ag _{0.75} InCl ₆	electron	11.54	62.43	765.15
	hole	9.78	62.43	31.98
Cs ₂ AgGa _{0.25} In _{0.75} Cl ₆	electron	11.47	66.75	804.62
	hole	10.36	66.75	59.06
Cs ₂ AgIr _{0.25} In _{0.75} Cl ₆	electron	11.53	72.08	673.36
	hole	8.57	72.08	88.10
Cs ₂ Zn _{0.50} Ag _{0.75} In _{0.75} Cl ₆	electron	11.38	58.97	672.35
	hole	10.31	58.97	53.86

between theory and experiment, Fröhlich's polaron model is observed to be a remarkable model. Using this model, here we have investigated the electron-phonon coupling in Cs₂AgInCl₆ and different alloyed compounds and estimated an upper limit on the related charge carrier mobilities. The dimensionless Fröhlich parameter α of dielectric electron-phonon coupling which can be seen as a comparative measure of Fröhlich coupling strength is given as

$$\alpha = \frac{1}{4\pi\epsilon_0} \frac{1}{2} \left(\frac{1}{\epsilon_\infty} - \frac{1}{\epsilon_{\text{static}}} \right) \frac{e^2}{\hbar\omega_{\text{LO}}} \left(\frac{2m^*\omega_{\text{LO}}}{\hbar} \right)^{1/2} \quad (6)$$

This parameter α is fully defined by the material specific properties, specifically, optical (ϵ_∞) and static (ϵ_{static}) dielectric constants, the carrier effective mass (m^*), and a characteristic phonon angular frequency (ω_{LO}). For a system with multiple phonon branches, an average LO frequency can be calculated by considering all the infrared active optical phonon branches and taking a spectral average of them³⁹. ϵ_0 is the permittivity of free space. We observe that due to an increase in high

Table 5: Polaron parameters corresponding to electrons in pristine Cs₂AgInCl₆ and different alloyed compounds.

Compounds	ω_{LO} (THz)	θ_{D} (K)	α_e	m_{P}/m^*	l_{P} (Å)	μ_{P} (cm ² V ⁻¹ s ⁻¹)
Cs ₂ AgInCl ₆	4.49	215	5.59	2.71	28.73	8.54
Cs ₂ AgInBr _{0.04} Cl _{5.96}	5.86	281	4.26	2.16	40.48	13.44
Cs ₂ AgInI _{0.04} Cl _{5.96}	5.85	280	3.48	1.88	45.09	21.42
Cs ₂ Au _{0.25} Ag _{0.75} InCl ₆	5.60	268	3.62	1.93	42.75	21.17
Cs ₂ Cu _{0.25} Ag _{0.75} InCl ₆	5.69	273	2.66	1.62	50.75	32.53
Cs ₂ AgGa _{0.25} In _{0.75} Cl ₆	5.36	257	3.54	1.90	41.85	20.81
Cs ₂ AgIr _{0.25} In _{0.75} Cl ₆	5.12	245	2.86	1.68	45.24	28.35
Cs ₂ Zn _{0.50} Ag _{0.75} In _{0.75} Cl ₆	3.07	147	4.13	2.11	25.56	21.60

frequency dielectric constant, the Fröhlich scattering strength in alloyed compounds is reduced (see Table 5). Note that, the value of α remains in the moderate strength range, and comparable to the hybrid halide perovskite series⁴⁰. Further, the Debye temperature (θ_{D}) of effective LO frequency comes out to be 215 K for pristine Cs₂AgInCl₆. Similarly, for the different alloyed systems as well, the Debye temperature is well below the room temperature and hence, suggests dominant polaronic contribution to limit carrier mobility near room temperature.

From the above discussion, we have found that these materials possess large dielectric electron-phonon coupling. Polarons are dressed quasiparticles, which are formed due to the interaction of electron and hole with the lattice. Within Fröhlich's polaron theory, as extended by Feynman, the polaron mass renormalisation for polaron, m_{P} ⁴¹ can be calculated as

$$m_{\text{P}} = m^* \left(1 + \frac{\alpha}{6} + \frac{\alpha^2}{40} \right) \quad (7)$$

Further, the polaron radius can be calculated as

$$l_{\text{P}} = \sqrt{\frac{h}{2cm^*\omega_{\text{LO}}}} \quad (8)$$

where, c is the speed of light. Our calculated polaron mass renormalisation and the corresponding

polaron radius are listed in Table 5. Notably, these parameters can be used to estimate an upper limit on charge carrier mobilities under the assumption that carriers are interacting only with the optical phonons. Now, the polaron mobility according to the Hellwarth polaron model³⁹ is defined as follows:

$$\mu_{\text{P}} = \frac{(3\sqrt{\pi}e)}{2\pi c\omega_{\text{LO}}m^*\alpha} \frac{\sinh(\beta/2)}{\beta^{5/2}} \frac{w^3}{v^3} \frac{1}{K} \quad (9)$$

where, $\beta = hc\omega_{\text{LO}}/k_{\text{B}}T$, w and v correspond to temperature dependent variational parameters. K is a function of v , w , and β . Here, we have calculated w and v by minimizing the free polaron energy (see section V in SI for details). The obtained upper limits on the charge carrier mobilities at room temperature are listed in Table 5. From Table 5, one can find that in case of pristine $\text{Cs}_2\text{AgInCl}_6$ and different alloyed compounds, large polarons [$l_{\text{P}} \gg$ lattice parameter] will be formed. This leads to increased carrier lifetime due to the reduction in carrier-carrier and carrier-defect scatterings⁴². Large polarons can be effectively seen as quasicharge carriers possessing higher effective masses than the original carriers, thus practically reducing the carrier mobility. In case of pristine $\text{Cs}_2\text{AgInCl}_6$, our estimated polaron mobility is $8.54 \text{ cm}^2\text{V}^{-1}\text{s}^{-1}$, which suggests the dominant role of electron-phonon coupling here. We have also found polaronic mass to be 2.71 times of the effective mass of electron, which confirms the increased carrier lattice interaction. Further, in case of alloyed compounds, we have observed substantial reduction in electronic effective mass and polaronic mass renormalization (see Table 5). As such, the limit to the electron mobility increases almost 2-4 times, in case of alloyed compounds. We have discussed the hole mobility as well (for reference, see SI section VI). From the above discussion, we infer that the reduction in effective mass and increase in dielectric constant will largely improve the carrier mobility and ensure a better screening against ionized impurities in different alloyed compounds compared to pristine $\text{Cs}_2\text{AgInCl}_6$. This shows the higher overall carrier mobility in different alloyed compounds.

In summary, using first-principles calculation, the excitonic, and polaronic properties of pristine $\text{Cs}_2\text{AgInCl}_6$ and different alloyed double perovskites are investigated systematically. Initially,

using Wannier-Mott approach, we have computed the upper and lower bound of exciton binding energy. After that, from the exciton lifetime calculation, we have found that the alloyed compounds have longer exciton lifetime than the pristine $\text{Cs}_2\text{AgInCl}_6$. Further, the deformation potential approach reveals substantial increase in the charge carrier mobility on alloying. Using the Feynman polaron model, we have discussed the carrier-lattice interaction in these materials. Careful analysis of carrier effective mass, electronic and ionic dielectric constant and effective LO frequency help us to address the electron-phonon coupling. The detailed theoretical investigation presented in this work will surely help the future studies to improve the overall performance of double perovskites.

Computational Methods

The density functional theory (DFT)^{43,44} calculations have been performed using the Vienna *ab initio* simulation package (VASP)^{45,46}. The ion-electron interactions in all the elemental constituents are described using projector-augmented wave (PAW) potentials^{46,47}. The double perovskite $\text{Cs}_2\text{AgInCl}_6$ has a cubic structure with space group $Fm\bar{3}m$. The corresponding sublattice is composed of alternate octahedra of InCl_6 and AgCl_6 as shown in Fig. 1(a). All the structures are optimized (the atomic positions are relaxed) using generalized gradient approximation of PBE⁴⁸ as the exchange-correlation (xc) functional until the forces are smaller than $0.001 \text{ eV}/\text{\AA}$. The electronic self consistency loop convergence is set to 0.01 meV , and the kinetic energy cutoff is set to 600 eV for plane wave basis set expansion. A k -grid of $4 \times 4 \times 4$ is used for Brillouin zone integration, which is generated using Monkhorst-Pack⁴⁹ scheme. Advanced hybrid xc functional HSE06⁵⁰ is used for the better estimation of band gap. For determination of optical properties, single shot GW (G_0W_0)^{51,52} calculations have been performed on top of the orbitals obtained from HSE06 xc functional. The polarizability calculations are carried out on a grid of 50 frequency points. The number of bands is set to four times the number of occupied orbitals. Note that spin orbit coupling was not taken into consideration here because it negligibly affects the electronic structures of Ag/In halide double perovskites^{25,53}. The ionic contribution to dielectric function has

been calculated using density functional perturbation theory (DFPT)⁵⁴ with $7 \times 7 \times 7$ k -grid. Carrier mobilities are simulated via implementing a temperature dependent Feynman polaron model⁵⁵. A detailed description of the model along with the necessary parameters needed can be found in Ref^{55–57}.

Acknowledgement

MJ acknowledges CSIR, India, for the senior research fellowship [grant no. 09/086(1344)/2018-EMR-I]. MK acknowledges CSIR, India, for the senior research fellowship [grant no. 09/086(1292)/2017-EMR-I]. PB acknowledges UGC, India, for the senior research fellowship [1392/(CSIR-UGC NET JUNE 2018)]. SB acknowledges the financial support from SERB under core research grant (grant no. CRG/2019/000647). We acknowledge the High Performance Computing (HPC) facility at IIT Delhi for computational resources.

Supporting Information Available

Electronic bandstructure of different alloyed compounds using $G_0W_0@HSE06$; Free charge carrier mobility using deformation potential model; Comparison of charge carrier mobility using PBE and HSE06 exchange-correlation (xc) functional; Deformation potential constant (E_l) and 3D elastic constant (C_{3D}) for alloyed compounds; Polaron mobility using Feynman polaron model; Polaron parameters for holes.

References

- (1) de Arquer, F. P. G.; Armin, A.; Meredith, P.; Sargent, E. H. Solution-processed semiconductors for next-generation photodetectors. *Nature Reviews Materials* **2017**, *2*, 1–17.

- (2) Kovalenko, M. V.; Protesescu, L.; Bodnarchuk, M. I. Properties and potential optoelectronic applications of lead halide perovskite nanocrystals. *Science* **2017**, *358*, 745–750.
- (3) Zhou, Y.; Chen, J.; Bakr, O. M.; Sun, H.-T. Metal-doped lead halide perovskites: synthesis, properties, and optoelectronic applications. *Chemistry of Materials* **2018**, *30*, 6589–6613.
- (4) Zhao, Y.; Zhu, K. Organic–inorganic hybrid lead halide perovskites for optoelectronic and electronic applications. *Chemical Society Reviews* **2016**, *45*, 655–689.
- (5) Yang, D.; Yang, R.; Wang, K.; Wu, C.; Zhu, X.; Feng, J.; Ren, X.; Fang, G.; Priya, S.; Liu, S. F. High efficiency planar-type perovskite solar cells with negligible hysteresis using EDTA-complexed SnO₂. *Nature communications* **2018**, *9*, 1–11.
- (6) Feng, J.; Zhu, X.; Yang, Z.; Zhang, X.; Niu, J.; Wang, Z.; Zuo, S.; Priya, S.; Liu, S.; Yang, D. Record efficiency stable flexible perovskite solar cell using effective additive assistant strategy. *Advanced Materials* **2018**, *30*, 1801418.
- (7) Cho, K. T.; Paek, S.; Grancini, G.; Roldán-Carmona, C.; Gao, P.; Lee, Y.; Nazeeruddin, M. K. Highly efficient perovskite solar cells with a compositionally engineered perovskite/hole transporting material interface. *Energy & Environmental Science* **2017**, *10*, 621–627.
- (8) Tan, Z.-K.; Moghaddam, R. S.; Lai, M. L.; Docampo, P.; Higler, R.; Deschler, F.; Price, M.; Sadhanala, A.; Pazos, L. M.; Credgington, D. et al. Bright light-emitting diodes based on organometal halide perovskite. *Nature nanotechnology* **2014**, *9*, 687–692.
- (9) Jain, M.; Singh, A.; Basera, P.; Kumar, M.; Bhattacharya, S. Understanding the role of Sn substitution and Pb-Vac in enhancing the optical properties and solar cell efficiency of CH(NH₂)₂Pb_{1-x-y}Sn_xVac_yBr₃. *J. Mater. Chem. C* **2020**, *8*, 10362–10368.
- (10) Kojima, A.; Teshima, K.; Shirai, Y.; Miyasaka, T. Organometal Halide Perovskites as Visible-Light Sensitizers for Photovoltaic Cells. *Journal of the American Chemical Society* **2009**, *131*, 6050–6051.

- (11) National Renewable Energy Laboratory (NREL) Best Research-Cell Efficiency Chart. <https://www.nrel.gov/pv/cell-efficiency.html>, accessed: January 26, 2021.
- (12) Zhao, B.; Bai, S.; Kim, V.; Lamboll, R.; Shivanna, R.; Auras, F.; Richter, J. M.; Yang, L.; Dai, L.; Alsari, M. et al. High-efficiency perovskite–polymer bulk heterostructure light-emitting diodes. *Nature Photonics* **2018**, *12*, 783–789.
- (13) Xiang, S.; Fu, Z.; Li, W.; Wei, Y.; Liu, J.; Liu, H.; Zhu, L.; Zhang, R.; Chen, H. Highly air-stable carbon-based α -CsPbI₃ perovskite solar cells with a broadened optical spectrum. *ACS Energy Letters* **2018**, *3*, 1824–1831.
- (14) McClure, E. T.; Ball, M. R.; Windl, W.; Woodward, P. M. Cs₂AgBiX₆ (X= Br, Cl): new visible light absorbing, lead-free halide perovskite semiconductors. *Chemistry of Materials* **2016**, *28*, 1348–1354.
- (15) Slavney, A. H.; Hu, T.; Lindenberg, A. M.; Karunadasa, H. I. A bismuth-halide double perovskite with long carrier recombination lifetime for photovoltaic applications. *Journal of the American chemical society* **2016**, *138*, 2138–2141.
- (16) Giustino, F.; Snaith, H.; Haghighirad, A. A.; Volonakis, G.; Filip, M.; Sakai, N.; Wenger, B. Lead-free halide double perovskites via heterovalent substitution of noble metals. *Journal of Physical Chemistry Letters* **2016**, *7*.
- (17) Filip, M. R.; Liu, X.; Miglio, A.; Hautier, G.; Giustino, F. Phase diagrams and stability of lead-free halide double perovskites Cs₂BB'X₆: B= Sb and Bi, B'= Cu, Ag, and Au, and X= Cl, Br, and I. *The Journal of Physical Chemistry C* **2018**, *122*, 158–170.
- (18) Schade, L.; Wright, A. D.; Johnson, R. D.; Dollmann, M.; Wenger, B.; Nayak, P. K.; Prabhakaran, D.; Herz, L. M.; Nicholas, R.; Snaith, H. J. et al. Structural and optical properties of Cs₂AgBiBr₆ double perovskite. *ACS Energy Letters* **2018**, *4*, 299–305.

- (19) Volonakis, G.; Haghghirad, A. A.; Milot, R. L.; Sio, W. H.; Filip, M. R.; Wenger, B.; Johnston, M. B.; Herz, L. M.; Snaith, H. J.; Giustino, F. Cs₂InAgCl₆: a new lead-free halide double perovskite with direct band gap. *The journal of physical chemistry letters* **2017**, *8*, 772–778.
- (20) Filip, M. R.; Hillman, S.; Haghghirad, A. A.; Snaith, H. J.; Giustino, F. Band gaps of the lead-free halide double perovskites Cs₂BiAgCl₆ and Cs₂BiAgBr₆ from theory and experiment. *The journal of physical chemistry letters* **2016**, *7*, 2579–2585.
- (21) Zhang, P.; Yang, J.; Wei, S.-H. Manipulation of cation combinations and configurations of halide double perovskites for solar cell absorbers. *Journal of Materials Chemistry A* **2018**, *6*, 1809–1815.
- (22) Sun, Q.; Yin, W.-J.; Wei, S.-H. Searching for stable perovskite solar cell materials using materials genome techniques and high-throughput calculations. *J. Mater. Chem. C* **2020**, *8*, 12012–12035.
- (23) Giorgi, G.; Yamashita, K.; Palummo, M. Two-dimensional optical excitations in the mixed-valence Cs₂Au₂I₆ fully inorganic double perovskite. *J. Mater. Chem. C* **2018**, *6*, 10197–10201.
- (24) Ning, W.; Wang, F.; Wu, B.; Lu, J.; Yan, Z.; Liu, X.; Tao, Y.; Liu, J.-M.; Huang, W.; Fahlman, M. et al. Long Electron–Hole Diffusion Length in High-Quality Lead-Free Double Perovskite Films. *Advanced Materials* **2018**, *30*, 1706246.
- (25) Tran, T. T.; Panella, J. R.; Chamorro, J. R.; Morey, J. R.; McQueen, T. M. Designing indirect-direct bandgap transitions in double perovskites. *Mater. Horiz.* **2017**, *4*, 688–693.
- (26) Luo, J.; Wang, X.; Li, S.; Liu, J.; Guo, Y.; Niu, G.; Yao, L.; Fu, Y.; Gao, L.; Dong, Q. et al. Efficient and stable emission of warm-white light from lead-free halide double perovskites. *Nature* **2018**, *563*, 541–545.

- (27) Zhou, J.; Xia, Z.; Molokeev, M. S.; Zhang, X.; Peng, D.; Liu, Q. Composition design, optical gap and stability investigations of lead-free halide double perovskite Cs₂AgInCl₆. *Journal of Materials Chemistry A* **2017**, *5*, 15031–15037.
- (28) Kumar, M.; Jain, M.; Singh, A.; Bhattacharya, S. Sublattice mixing in Cs₂AgInCl₆ for enhanced optical properties from first-principles. *Applied Physics Letters* **2021**, *118*, 021901.
- (29) Waters, M. J.; Hashemi, D.; Kieffer, J. Semiclassical model for calculating exciton and polaron pair energetics at interfaces. *Materials Science and Engineering: B* **2020**, *261*, 114657.
- (30) Volonakis, G.; Filip, M. R.; Haghghirad, A. A.; Sakai, N.; Wenger, B.; Snaith, H. J.; Giustino, F. Lead-free halide double perovskites via heterovalent substitution of noble metals. *The journal of physical chemistry letters* **2016**, *7*, 1254–1259.
- (31) Freysoldt, C.; Grabowski, B.; Hickel, T.; Neugebauer, J.; Kresse, G.; Janotti, A.; Van de Walle, C. G. First-principles calculations for point defects in solids. *Reviews of modern physics* **2014**, *86*, 253.
- (32) Bokdam, M.; Sander, T.; Stroppa, A.; Picozzi, S.; Sarma, D.; Franchini, C.; Kresse, G. Role of polar phonons in the photo excited state of metal halide perovskites. *Scientific reports* **2016**, *6*, 1–8.
- (33) Manna, D.; Kangsabanik, J.; Das, T. K.; Das, D.; Alam, A.; Yella, A. Lattice Dynamics and Electron–Phonon Coupling in Lead-Free Cs₂AgIn_{1-x}Bi_xCl₆ Double Perovskite Nanocrystals. *The journal of physical chemistry letters* **2020**, *11*, 2113–2120.
- (34) Selig, M.; Berghäuser, G.; Raja, A.; Nagler, P.; Schüller, C.; Heinz, T. F.; Korn, T.; Chernikov, A.; Malic, E.; Knorr, A. Excitonic linewidth and coherence lifetime in monolayer transition metal dichalcogenides. *Nature communications* **2016**, *7*, 1–6.
- (35) Bardeen, J.; Shockley, W. Deformation potentials and mobilities in non-polar crystals. *Physical review* **1950**, *80*, 72.

- (36) Zhang, Z.; Su, J.; Hou, J.; Lin, Z.; Hu, Z.; Chang, J.; Zhang, J.; Hao, Y. Potential Applications of Halide Double Perovskite Cs₂AgInX₆ (X = Cl, Br) in Flexible Optoelectronics: Unusual Effects of Uniaxial Strains. *The Journal of Physical Chemistry Letters* **2019**, *10*, 1120–1125.
- (37) Fröhlich, H. Electrons in lattice fields. *Advances in Physics* **1954**, *3*, 325–361.
- (38) Herz, L. M. Charge-carrier mobilities in metal halide perovskites: fundamental mechanisms and limits. *ACS Energy Letters* **2017**, *2*, 1539–1548.
- (39) Hellwarth, R. W.; Biaggio, I. Mobility of an electron in a multimode polar lattice. *Physical Review B* **1999**, *60*, 299.
- (40) Jain, M.; Gill, D.; Bhumla, P.; Basera, P.; Bhattacharya, S. Theoretical insights to excitonic effect in lead bromide perovskites. *Applied Physics Letters* **2021**, *118*, 192103.
- (41) Feynman, R. P. Slow electrons in a polar crystal. *Physical Review* **1955**, *97*, 660.
- (42) Zheng, F.; Wang, L.-w. Large polaron formation and its effect on electron transport in hybrid perovskites. *Energy & Environmental Science* **2019**, *12*, 1219–1230.
- (43) Hohenberg, P.; Kohn, W. Inhomogeneous Electron Gas. *Phys. Rev.* **1964**, *136*, B864–B871.
- (44) Kohn, W.; Sham, L. J. Self-Consistent Equations Including Exchange and Correlation Effects. *Phys. Rev.* **1965**, *140*, A1133–A1138.
- (45) Kresse, G.; Furthmüller, J. Efficiency of ab-initio total energy calculations for metals and semiconductors using a plane-wave basis set. *Computational Materials Science* **1996**, *6*, 15–50.
- (46) Kresse, G.; Joubert, D. From ultrasoft pseudopotentials to the projector augmented-wave method. *Phys. Rev. B* **1999**, *59*, 1758–1775.
- (47) Blöchl, P. E. Projector augmented-wave method. *Phys. Rev. B* **1994**, *50*, 17953–17979.

- (48) Perdew, J. P.; Burke, K.; Ernzerhof, M. Generalized Gradient Approximation Made Simple. *Phys. Rev. Lett.* **1996**, *77*, 3865–3868.
- (49) Monkhorst, H. J.; Pack, J. D. Special points for Brillouin-zone integrations. *Phys. Rev. B* **1976**, *13*, 5188–5192.
- (50) Krukau, A. V.; Vydrov, O. A.; Izmaylov, A. F.; Scuseria, G. E. Influence of the exchange screening parameter on the performance of screened hybrid functionals. *The Journal of Chemical Physics* **2006**, *125*, 224106.
- (51) Hedin, L. New Method for Calculating the One-Particle Green's Function with Application to the Electron-Gas Problem. *Phys. Rev.* **1965**, *139*, A796–A823.
- (52) Hybertsen, M. S.; Louie, S. G. First-Principles Theory of Quasiparticles: Calculation of Band Gaps in Semiconductors and Insulators. *Phys. Rev. Lett.* **1985**, *55*, 1418–1421.
- (53) Cai, Y.; Xie, W.; Teng, Y. T.; Harikesh, P. C.; Ghosh, B.; Huck, P.; Persson, K. A.; Mathews, N.; Mhaisalkar, S. G.; Sherburne, M. et al. High-throughput Computational Study of Halide Double Perovskite Inorganic Compounds. *Chemistry of Materials* **2019**, *31*, 5392–5401.
- (54) Gajdoš, M.; Hummer, K.; Kresse, G.; Furthmüller, J.; Bechstedt, F. Linear optical properties in the projector-augmented wave methodology. *Physical Review B* **2006**, *73*, 045112.
- (55) Feynman, R. P.; Hellwarth, R. W.; Iddings, C. K.; Platzman, P. M. Mobility of Slow Electrons in a Polar Crystal. *Phys. Rev.* **1962**, *127*, 1004–1017.
- (56) Frost, J. M. Calculating polaron mobility in halide perovskites. *Phys. Rev. B* **2017**, *96*, 195202.
- (57) Kadanoff, L. P. Boltzmann Equation for Polarons. *Phys. Rev.* **1963**, *130*, 1364–1369.

Lead Free Alloyed Double Perovskites: An Emerging Class of Materials from Many-Body Perturbation Theory

Manjari Jain,^{*} Manish Kumar, Preeti Bhumla, and Saswata Bhattacharya^{*}

Department of Physics, Indian Institute of Technology Delhi, New Delhi, India

E-mail: Manjari.Jain@physics.iitd.ac.in[MJ]; saswata@physics.iitd.ac.in[SB]

Phone: +91-11-2659 1359. Fax: +91-11-2658 2037

Supplemental Material

- I. Electronic bandstructure of different alloyed compounds using $G_0W_0@HSE06$.
- II. Free charge carrier mobility using deformation potential model.
- III. Comparison of charge carrier mobility using PBE and HSE06 exchange-correlation (xc) functional.
- IV. Deformation potential constant (E_l) and 3D elastic constant (C_{3D}) for alloyed compounds.
- V. Polaron mobility using Feynman polaron model.
- VI. Polaron parameters for holes.

I. Electronic bandstructure of different alloyed compounds using $G_0W_0@HSE06$

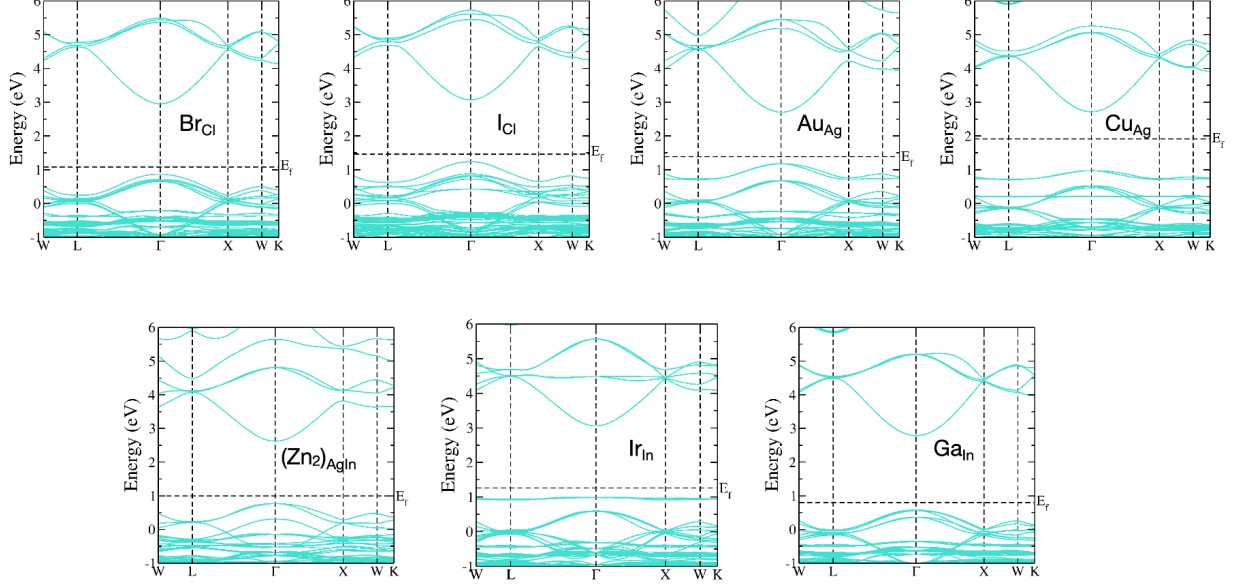


Figure S1: Electronic bandstructure of different alloyed compounds. E_f is the fermi energy level.

II. Free charge carrier mobility using deformation potential model

According to deformation potential model,¹ the carrier mobility is defined as:

$$\mu = \frac{2\sqrt{2}\pi e\hbar^4 C_{3D}}{3(k_B T)^{3/2} (m^*)^{5/2} E_l^2} \quad (1)$$

where k_B , T , and m^* correspond to the Boltzmann constant, temperature, and effective mass, respectively. Here, we have performed the calculations at 300 K temperature. In the above

equation, E_l corresponds to the deformation potential constant along z-direction for electron and hole. It is given by:

$$E_l = \frac{\Delta E_i}{\Delta l/l_0} \quad (2)$$

where, ΔE_i denotes the change in the energy or shift in the position of VBM or CBm under uniaxial strain along the z-direction. l_0 is the lattice constant along the transport direction (z-axis). Δl denotes the change or deformation in the lattice constant l_0 on application of uniaxial strain. The elastic modulus C_{3D} is computed using the relation $(E - E_0)/V_0 = C(\Delta l/l_0)^2/2$, where E_0 and E are the total energies of undeformed and deformed system, respectively. V_0 represents the equilibrium volume of the system. Note, herein, we have chosen strain range from -1.0% to +1.0% to obtain the fitted values of C_{3D} and E_l .

III. Comparison of charge carrier mobility using PBE and HSE06 exchange-correlation (xc) functional

Table S1: Calculated deformation potential constant (E_l), 3D elastic constant (C_{3D}), carrier mobility (μ) for holes along the transport direction (z-axis) of pristine $\text{Cs}_2\text{AgInCl}_6$ and $\text{Cs}_2\text{Cu}_{0.25}\text{Ag}_{0.75}\text{InCl}_6$ at 300 K.

Compounds	PBE			HSE06		
	E_l (eV)	C_{3D} (Nm^{-2})	μ ($\text{cm}^2\text{V}^{-1}\text{s}^{-1}$)	E_l (eV)	C_{3D} (Nm^{-2})	μ ($\text{cm}^2\text{V}^{-1}\text{s}^{-1}$)
$\text{Cs}_2\text{AgInCl}_6$	10.66	67.48	30.68	10.81	70.54	31.23
$\text{Cs}_2\text{Cu}_{0.25}\text{Ag}_{0.75}\text{InCl}_6$	10.36	62.43	31.98	9.51	65.09	35.55

As we can see from Table S1, the carrier mobilities calculated using PBE² and HSE06³ xc functional are quite comparable. Therefore, we have proceeded with PBE functional as it is cost effective.

IV. Deformation potential constant (E_l) and 3D elastic constant (C_{3D}) for alloyed compounds

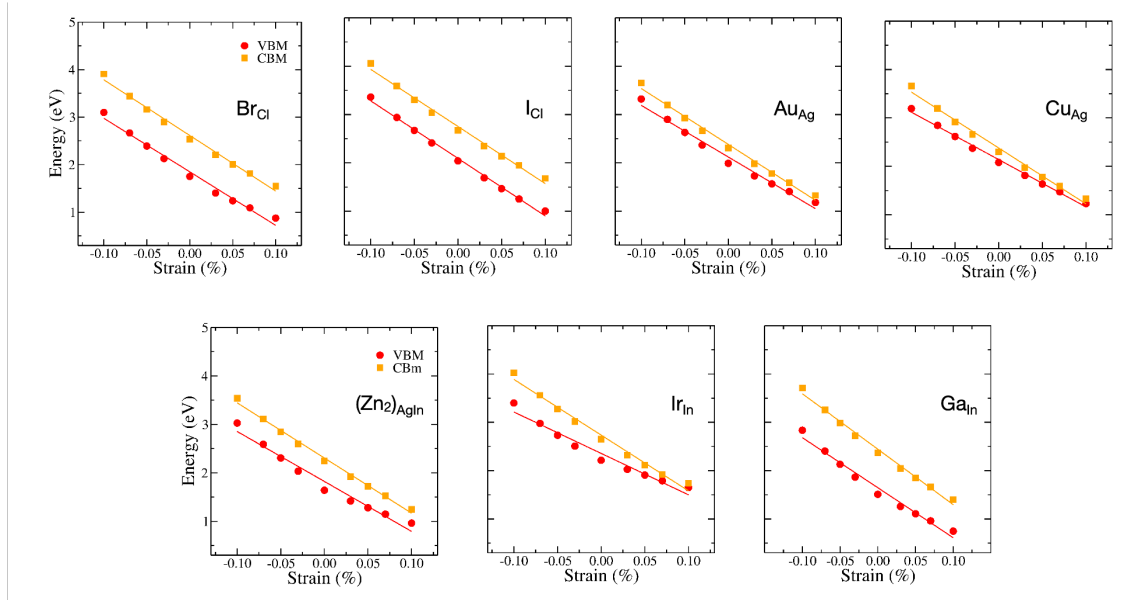


Figure S2: Energy shifts of CBm and VBM of different alloyed compounds under strain. The slopes of these lines are the corresponding deformation potential.

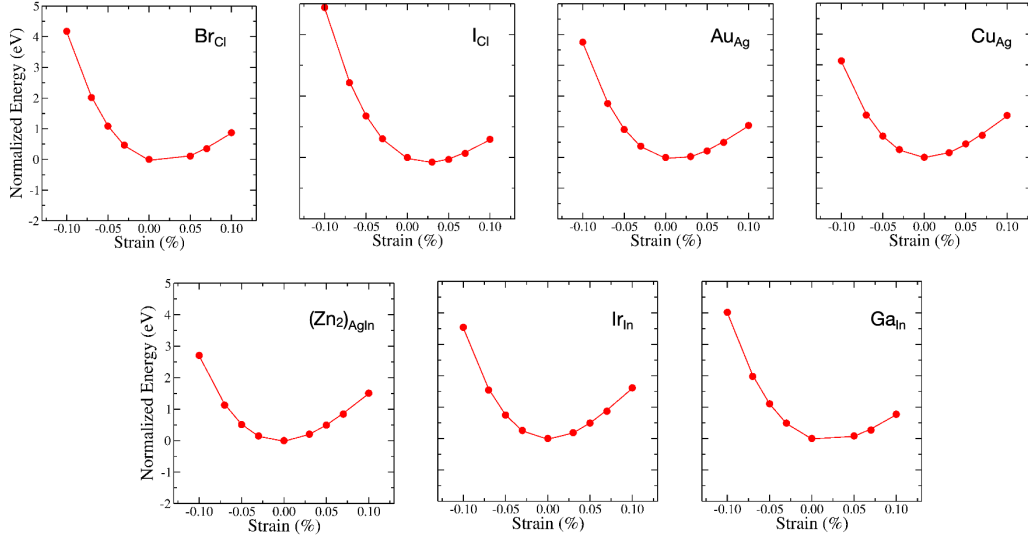


Figure S3: Relationship between total energy and the applied strain. The quadratic fitting of the data gives the elastic constant of different alloyed compounds.

V. Polaron mobility using Feynman polaron model

Polaron mobility according to the Hellwarth polaron model⁴ is defined as follows:

$$\mu_P = \frac{(3\sqrt{\pi}e)}{2\pi c\omega_{LO}m^*\alpha} \frac{\sinh(\beta/2)}{\beta^{5/2}} \frac{w^3}{v^3} \frac{1}{K} \quad (3)$$

where, $\beta = hc\omega_{LO}/k_B T$, e is the electronic charge, m^* is the effective mass of charge carrier, w and v correspond to temperature dependent variational parameters. K is a function of v , w , and β defined as follows:

$$K(a, b) = \int_0^\infty du [u^2 + a^2 - b\cos(vu)]^{-3/2} \cos(u) \quad (4)$$

In the above equation, a^2 and b can be calculated using following formulas:

$$a^2 = (\beta/2)^2 + \frac{(v^2 - w^2)}{w^2 v} \beta \coth(\beta v/2) \quad (5)$$

$$b = \frac{(v^2 - w^2)}{w^2 v} \frac{\beta}{\sinh(\beta v/2)} \quad (6)$$

VI. Polaron parameters for holes

Table S2: Polaron parameters corresponding to holes in pristine Cs₂AgInCl₆ and different alloyed compounds.

Compounds	ω_{LO} (THz)	θ_{D} (K)	α_{h}	m_{P}/m^*	l_{P} (Å)	μ_{P} (cm ² V ⁻¹ s ⁻¹)
Cs ₂ AgInCl ₆	4.49	215	10.75	5.68	19.07	0.29
Cs ₂ AgInBr _{0.04} Cl _{5.96}	5.86	281	7.21	3.50	29.86	1.22
Cs ₂ AgInI _{0.04} Cl _{5.96}	5.85	280	5.59	2.71	34.79	3.03
Cs ₂ Au _{0.25} Ag _{0.75} InCl ₆	5.60	268	6.47	3.12	30.92	1.75
Cs ₂ Cu _{0.25} Ag _{0.75} InCl ₆	5.69	273	5.36	2.61	34.93	2.11
Cs ₂ AgGa _{0.25} In _{0.75} Cl ₆	5.36	257	6.43	3.10	30.10	1.67
Cs ₂ AgIr _{0.25} In _{0.75} Cl ₆	5.12	245	4.92	2.42	33.91	3.49
Cs ₂ Zn _{0.50} Ag _{0.75} In _{0.75} Cl ₆	3.07	147	7.11	3.44	19.09	2.37

References

- (1) Bardeen, J.; Shockley, W. Deformation potentials and mobilities in non-polar crystals. *Physical review* **1950**, *80*, 72.
- (2) Perdew, J. P.; Burke, K.; Ernzerhof, M. Generalized Gradient Approximation Made Simple. *Phys. Rev. Lett.* **1996**, *77*, 3865–3868.
- (3) Krukau, A. V.; Vydrov, O. A.; Izmaylov, A. F.; Scuseria, G. E. Influence of the exchange screening parameter on the performance of screened hybrid functionals. *The Journal of Chemical Physics* **2006**, *125*, 224106.
- (4) Hellwarth, R. W.; Biaggio, I. Mobility of an electron in a multimode polar lattice. *Physical Review B* **1999**, *60*, 299.